Fire Technology (2026) 62:158
https://doi.org/10.1007/s10694-026-01989-x

Analysis of Thermohydraulic Spalling in Blended Cement Concrete

Tim Pittrich[1,2] · Frank Dehn[2] · Frank Weise[1] · Ludwig Stelzner[1]

Received: 30 November 2025 / Revised: 17 July 2026 / Accepted: 9 August 2026

Abstract
Recently, the construction industry has increasingly focused on the development of more sustainable transport infrastructure, such as tunnels, driven by the growing use of clinker-reduced cements. One major challenge in this context is fire exposure, which can lead to severe structural damage through concrete spalling, thereby compromising the integrity of the structure. To date, the fire-induced spalling behavior of blended cement concrete remains insufficiently understood. This is particularly concerning, given the increasing adoption of blended cements with reduced clinker content, which are expected to see widespread use in the future. Consequently, a deeper understanding of how different cement types influence spalling susceptibility is of great importance. A comprehensive study was conducted to investigate spalling behavior and analyze the associated thermo-hydraulic effects in concretes made with CEM I, CEM II/A-LL, CEM III/A, and CEM II/B-Q. The findings revealed that the use of blended cements generally led to increased spalling susceptibility, even in normal-strength concrete. Additional analysis indicated that blended cement concretes exhibited lower permeability and higher moisture content, both of which are likely contributors to the elevated spalling risk. Furthermore, the study showed that moisture transport during heating closely follows the dehydration behavior of the cementitious matrix. Blended cement pastes were found to contain lower quantities of early-dehydrating AFt and AFm phases, as well as more thermally stable C-(A)-S-H phases. Moreover, the incorporation of polypropylene fibers into the concrete mix effectively mitigated spalling across all cement types. Therefore, demonstrating the continued effectiveness of polypropylene fibers as a spalling prevention strategy.

Keywords Fire induced spalling · Blended cement · SCM · Moisture transport · Dehydration · PP fibers

1 Introduction

The maintenance and expansion of transport infrastructure form the backbone of any economy. This applies not only to various types of transport routes and bridge structures but also to tunnel systems. However, the rise in traffic volume, vehicle speeds, and the expanding

Extended author information available on the last page of the article

Published online: 22 August 2026

size of tunnels also heightens the risk of tunnel fires [1]. These fires can have devastating consequences due to the rapid heat development in such confined environments. Beyond the threat to human life, tunnel fires can cause severe structural damage, primarily due to the loss of reinforced concrete strength at elevated temperatures and the occurrence of spalling. The latter results in the loss of the concrete cover, thereby exposing the steel reinforcement directly to high temperatures. This exposure causes further significant strength degradation and ultimately compromises the structural integrity of the tunnel. This not only leads to high repair costs but also results in significant economic losses due to prolonged tunnel closures.

At the same time, the concrete industry is already responsible for approximately 6–7% of global CO_2 emissions, with around 5% attributed to Portland cement production alone [2]. As the demand for infrastructure continues to grow, more sustainable alternatives are urgently needed to reduce the environmental impact of the construction sector. Roughly two-thirds of the CO_2 emissions from Portland cement production stem from the decomposition of limestone, a process that remains unavoidable, even in technologically optimized cement plants. Consequently, reducing the clinker factor is considered one of the most effective strategies for producing greener cement [2]. This can be achieved by partially replacing cement clinker with supplementary cementitious materials (SCMs) such as fly ash, blast furnace slag, or limestone to create blended cements. However, the long-term availability of fly ash and slag is uncertain, highlighting the need for viable alternatives. Calcined clays show great promise in this regard due to their global abundance, excellent pozzolanic properties, and significantly lower CO_2 emissions during production [3].

With the increasing variety of SCMs and the growing use of blended cements in practice, understanding their behavior under fire exposure is of great importance to ensure the continued safety and resilience of infrastructure. Against this background a comprehensive study regarding the spalling behavior with subsequent analysis of the thermohydraulic influences was carried out (see Fig. 1). The work of this project included a detailed literature review, in-depth fire spalling tests, investigations of the thermally induced moisture trans-

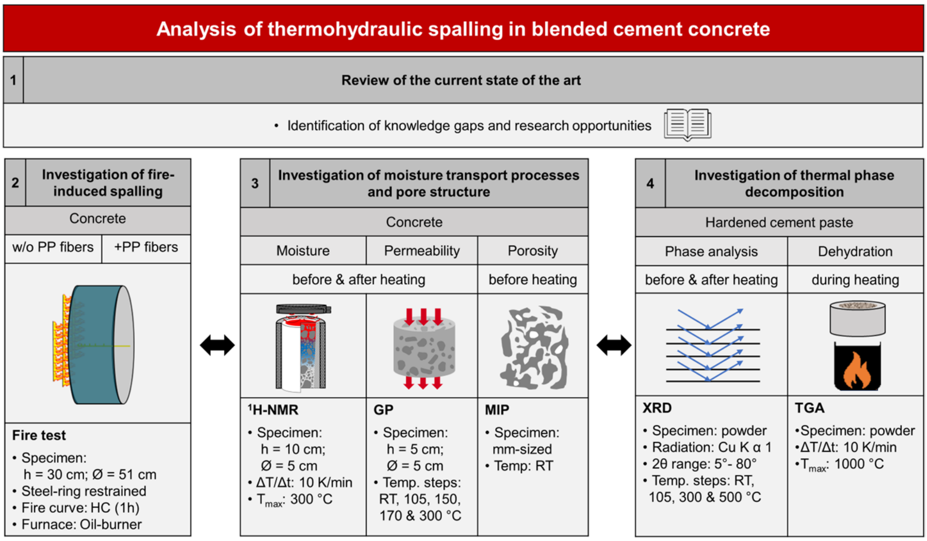

Fig. 1 Research program

port processes by hydrogen proton nuclear magnetic resonance (^{1}H-NMR) relaxometry, determination of gas permeability (GP) as well as the analysis of the pore structure by mercury intrusion porosimeter (MIP). Moreover, decomposition and dehydration behavior of hardened blended cement pastes were studied by X-ray diffraction (XRD) and thermal gravimetric analysis (TGA).

2 State of the Art

The concept of a thermohydraulic spalling mechanism in concrete was first introduced by Shorter and Harmathy in 1961 [4]. The authors stated that during fire exposure, the water within the concrete begins to evaporate, initiating pressure-driven moisture migration both towards the surface and deeper into the concrete element. Due to the temperature gradient established across the cross-section, water vapor condenses in the cooler interior, forming a saturated zone. As saturation increases, a so-called moisture clog develops, which impedes further moisture transport and leads to a buildup of pore pressure. If this pressure exceeds the tensile strength of the concrete, spalling occurs. However, the direct relationship between pore pressure and spalling has not been conclusively verified, as accurate pore pressure measurements during fire tests remain technically challenging. More recent studies suggest that the acceleration of concrete fragments may primarily influenced by initial microcracking and the associated adiabatic expansion of superheated water [5].

In addition to the thermohydraulic mechanism, which according to Bažant may act primarily as a trigger [6], thermomechanical mechanisms have also been identified as contributing factors to explosive spalling. Two primary sources of thermomechanical stress have been recognized. The first one deals with thermal mismatch between cement paste and aggregates. At approximately 150 °C, cement paste tends to shrink, while aggregates continue to expand [7]. This mismatch in thermal deformation induces internal stresses that can lead to microcracking, thereby promoting explosive spalling. The second one is based on restraint thermal dilations as the temperature gradient during fire exposure causes differential thermal expansion within the concrete cross-section. When this expansion is restrained by surrounding structural elements, compressive stresses develop parallel to the heated surface. These, in turn, generate transverse tensile stresses. If these stresses exceed the tensile strength of the concrete, spalling may occur [8, 9].

A commonly used mitigation strategy against spalling is the addition of Polypropylene fibers (PP fibers) to the concrete mixture. During a fire scenario the PP fibers melt around 160 °C which allows water vapor to escape through empty fiber channels and the developed microcrack network caused by the thermal expansion forces [10].

To understand the impact of blended cements on the fire-induced spalling behavior of concrete, the current state of the art was thoroughly reviewed in our previous paper [11]. It can be briefly concluded that the type of cement can significantly influence spalling behavior under fire exposure. Notably, the use of silica fume (SF) and metakaolin (MK) increases spalling susceptibility, primarily due to the formation of a very dense microstructure. Conversely, high amounts of FA (> 25%) tend to reduce the risk of spalling, while lower amounts show no consistent trend. For other supplementary cementitious materials and cement types, no definitive conclusions could be drawn, as existing results are marked by considerable uncertainty and contradiction. This is largely due to the limited number of

Table 1 Concrete composition

Component [kg/m³]	CEM I		CEM II/A-LL		CEM III/A		CEM II/B-Q	
	w/o PP	with PP	w/o PP	with PP	w/o PP	with PP	w/o PP	with PP
cement	420		420		420		420	
water (w/c)	197 (0.47)		197 (0.47)		197 (0.47)		197 (0.47)	
superplasticiser	0	1.5	0	3.4	0	2.1	2.5	5.0
PP fibers	0	2	0	2	0	2	0	2
quarzitic agg								
0/2 mm	646	640	646	634	640	637	634	628
2/4 mm	153	152	153	150	152	151	150	149
4/8 mm	221	219	221	217	219	218	217	215
8/16 mm	679	675	679	668	679	669	666	661

Table 2 Slump flow of the fresh concrete

	CEM I		CEM II/A-LL		CEM III/A		CEM II/B-Q	
	w/o PP	with PP	w/o PP	with PP	w/o PP	with PP	w/o PP	with PP
slump flow [mm]	445	395	395	500	418	455	390	465

studies that employed well-defined spalling experiments with suitable testing and evaluation protocols. Comparisons between different research groups were challenging due to variations in experimental setups and evaluation criteria. Moreover, no particular results regarding the influence of cement containing calcined clay existed up to this date even though they are forecast to be the leading SCM of the future.

3 Experimental Investigations

3.1 Fire-Induced Spalling

In the next phase of the study, in-depth spalling tests were conducted to gain further insight into the influence of blended cements on the spalling behavior of concrete. These tests and evaluation methods followed the RILEM Recommendations of RILEM TC 256-SPF [12, 13]. The key findings are summarized below the complete description of the testing set up and results can be found in [14].

Tunnel-grade normal strength concrete (NSC) was prepared using four different cement types in accordance with DIN EN197-1 [15]: Ordinary Portland cement CEM I 42.5 N as the reference, limestone cement CEM II/A-LL 42.5 N and slag cement CEM III/A 42.5 N representing current practice, and calcined clay cement CEM II/B-Q 42.5 N reflecting future trends. The exact chemical and mineralogical phase composition is reported in Pittrich et al. [16]. The concrete mix had a water-to-cement ratio (w/c) of 0.47 and included quarzitic aggregates. Although Eurocode 2 [17] does not prescribe specific measures against spalling for NSC, an additional mix was prepared for each concrete composition containing 2 kg/m³ of PP fibers (l = 6 mm; Ø = 15.4 μm) to evaluate their effectiveness in blended cement systems. All concrete compositions are given in Table 1. Because the inclusion of PP fibers significantly reduces concrete workability, higher amounts of superplasticizer were required to maintain consistency comparable to the fiber-free mixes (see Table 2). The specimens were demolded one day after casting and subsequently placed under water for 6 more days, afterwards the specimens were conditioned at (20 ± 2) °C and (65 ± 5) % RH until the day of testing (> 90 d). A steel-ring restrained test setup, similar to that used by Klimek et al. [18] based on the work of Ozawa et al. [19], was employed to simulate the behavior of a large-scale concrete element under fire exposure. During the fire tests, the 8 mm thick steel ring and the outer edge region of the specimen were kept thermally insulated. Thereby, the steel ring restrains the thermal expansion of the heated concrete core. As a result, compressive stresses developed perpendicular to the direction of fire exposure. The final test specimens had a diameter of 51 cm and a height of 30 cm.

Fire testing was carried out using a 1 m^3-furnace with two oil burners, applying the Hydrocarbon (HC) fire curve for a duration of one hour. For each concrete composition two tests were performed. During the experiment, video and audio recordings were made to count the spalling events. Temperature measurements were taken using embedded Type K thermocouples positioned at depths of 10, 20, 30, 50, and 100 mm in the center of the specimen. The specimen's topography was analyzed before and after the fire test with a 3D Laser scanner after all loose debris were removed. The scanners accuracy is specified as 20 µm + 35 µm/m, comprising a fixed base accuracy of 20 µm and an additional error of 35 µm per meter of measured length. Furthermore, the moisture content on the day of testing was determined by drying two cylindrical specimens (h = 30 cm; d = 10 cm) from the same production batch at 105 °C to constant mass. Constant mass was defined as a change in mass of ± 0.1 wt.-% within 24 h.

The results presented in Fig. 2 indicate a significant increase in spalling susceptibility across all types of blended cement concrete. In contrast, CEM I concrete exhibited minimal damage, with only five recorded spalling events and an average spalled volume of 1.5 vol.-%. CEM II/A-LL and CEM III/A showed notably higher levels of deterioration, each with an average of 83 and 111 spalling events and average spalled volumes of around 7 vol.-%. The most severe damage was observed in CEM II/B-Q concrete, which on average experienced 176 spalling events with a spalled volume exceeding 9 vol.-%. Of particular interest was the temperature development at a depth of 50 mm, where reinforcement layers are typically located (see Fig. 3). While CEM I concrete maintained temperatures around 400 °C, significantly higher temperatures were recorded for the blended cements: ca. 600 °C for CEM III/A, 700 °C for CEM II/A-LL, and above 1000 °C for CEM II/B-Q. These elevated temperatures are attributed to the absence of adequate concrete cover. Since temperatures above 500 °C can lead to a substantial reduction in the strength of reinforcing steel, this finding underscores the increased vulnerability of blended cement concretes under fire exposure. The most likely cause of this occurrence is the increased moisture content in blended cement concrete (see Fig. 2). Although these differences may seem minor, it was demonstrated by Maier et al. [20] that even slight increases in moisture can significantly raise spalling susceptibility. This critical finding must be carefully considered in the development of more sustainable concrete formulations in future construction.

However, with the addition of PP fibers no spalling was recorded in any specimen, concluding that the PP fibers are equally effective regardless of the cement type used. However, Fig. 3 shows local surface uplifts of up to 5 mm occurred, which can be attributed to crack formation within the specimens. Furthermore, it should be highlighted that the temperatures in 50 mm depth were similar for every concrete type with a maximum temperature after 60 min of fire exposure of around 200 °C (see Fig. 3), protecting a potential reinforcement

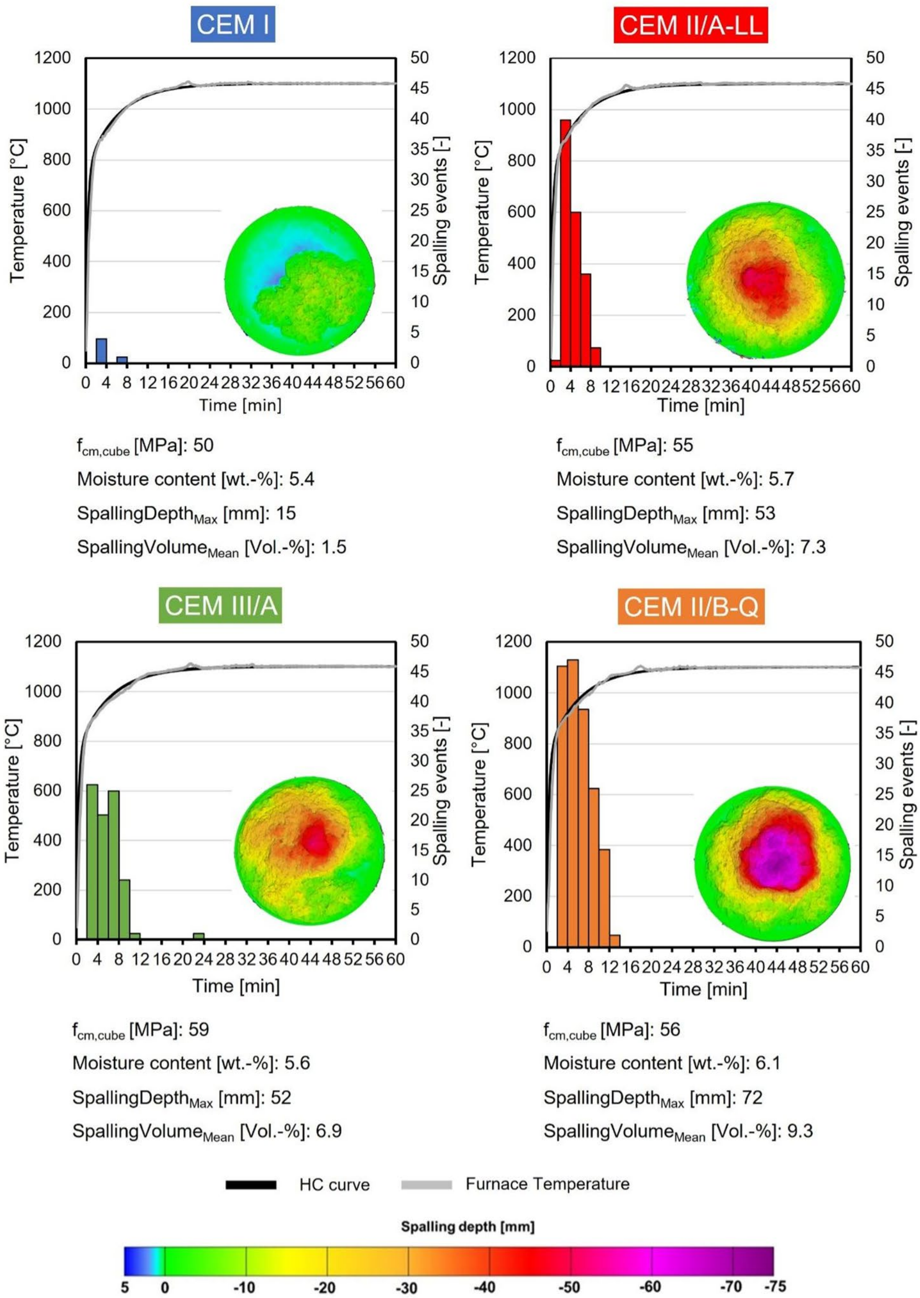

Fig. 2 Summary of the fire tests, showing the furnace temperature, the number of spalling events and the concrete properties in relation to the spalling volume and maximum spalling depth as mean values of two specimens. The 3D-scan represents one exemplary sample of each concrete type

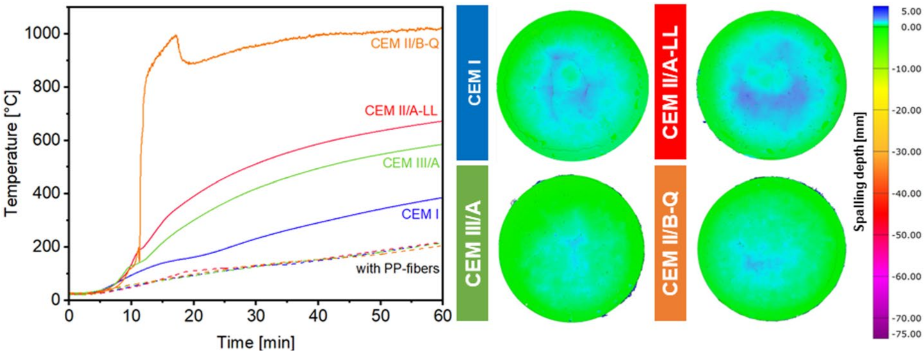

Fig. 3 Temperature development in 50 mm depth in the different concretes with and without PP fibers during fire exposure (left) and difference of the surface height distribution of the PP fiber-reinforced concrete specimens after fire exposure (right)

layer from direct flame exposure and consequent strength loss. Therefore, PP fibers remain a successful mitigation strategy.

3.2 Moisture Transport Processes and Pore Structure

The thermally induced moisture transport was analyzed to understand the reasons behind the different spalling behaviors found in the different types of blended cement concrete. ^{1}H-NMR relaxometry measurements were carried out before and after heating to obtain information about the pore size specific moisture distribution and the corresponding development of the moisture clog. The NMR-tomograph worked with a vertical resolution of 2 mm and was equipped with a 52 mm diameter radio-frequency coil. To enhance the decay of the transverse relaxation time (T_2), a Carr–Purcell–Meiboom–Gill (CPMG) pulse sequence was employed. The sequence used an echo time of 70 µs, generated 1429 echoes, and included 200 scans for each slice (for further details about the device see [21]). The inversion of the recorded signal was conducted with NUCLEUS a Matlab tool developed by Hiller and Costabel [22]. Additionally, supportive analysis in the form of GP and MIP measurements were conducted to receive further knowledge on the pore structure and transport properties. The main findings are presented below; further information and results can be found in [23].

The ^{1}H-NMR relaxometry measurements were conducted on small scale concrete cylinders cast in a Macor ceramic following the methodology of Stelzner et al. [24] for two samples of each concrete. First, pore size specific moisture distribution was determined before heating. Thereafter, the samples were exposed to one sided heating (10 K/min) until a surface temperature of 300 °C was reached and held constant for 40 more mins. Then, the samples were allowed to cool freely for 120 min and the pore size specific moisture distribution was determined again. It should be noted that measuring the moisture distribution in the cooled state may not fully reflect its distribution during heating. This discrepancy can result in deeper penetration of the drying front and less pronounced moisture clogging. Based on the numerical analysis reported in [23] it can be estimated that the shift in depth and moisture content between the end of heating and the measurement in the cooled state is within 10 mm and 1 vol.-%, respectively, for every concrete type. Nevertheless, the relative differences in drying behavior are still sufficiently accurately reflected in the measurements after cooling for the interpretation of the results. The temperature was recorded in accompanying specimens of the same kind in depths of 5 mm, 10 mm, 20 mm, 30 mm, 50 mm and 70 mm. In addition, the initial porosity was measured by means of MIP on small concrete fragments after [25]. The gas permeability measurements were carried out with Ar gas following pressure steps of 3,4 and 5 bar on accompanying cylindric samples (h = 5 cm; Ø = 5 cm) after exposure to 20, 105, 150, 170 and 300 °C according to [26]. Thereafter, the intrinsic gas permeability was determined after Klinkenberg [27].

The results in Fig. 4 clearly show a less pronounced initial drying gradient on the top and bottom in CEM III/A and CEM II/B-Q accompanied with a higher average moisture content of 13.4 and 13.2 vol.-% equal to 6.5 and 6.4 wt.-%. In comparison to 11.7 and 11.0 vol.-% equal to 5.7 and 5.3 wt.-% in CEM I and CEM II/A-LL concrete. In general, all samples have most of their water stored as gel pore water ($d_{Pore} \leq 10$ nm) and only minor fractions in capillary pore water ($d_{Pore} > 10$ nm). While CEM I and CEM II/A-LL show a quite equal moisture distribution, CEM III/A is exhibiting the most amount of capillary water and CEM II/B-Q the most amount of gel pore water. After high-temperature exposure the drying front and the subsequent appearance of the moisture clog were confirmed in every specimen. The onset of the moisture clog was defined here as the intersection between the initial water content prior to heating and the water content measured after heating. In particular, CEM II/B-Q showed the overall deepest sitting moisture clog. In addition, reconfiguration of the pore water from gel to capillary pores was recognized in all the samples leading to an overall increase in capillary pore water. In the area of the moisture clog the capillary pore water was now even the dominate fraction, except for CEM II-B-Q sample where the capillary pore water content never exceeds the gel pore water content. The effect of the PP fibers was noticeably detectable during the NMR measurements shown in Fig. 4. The results showed a slightly decreased moisture content in the PP fibers mixes in the initial state. After one-sided

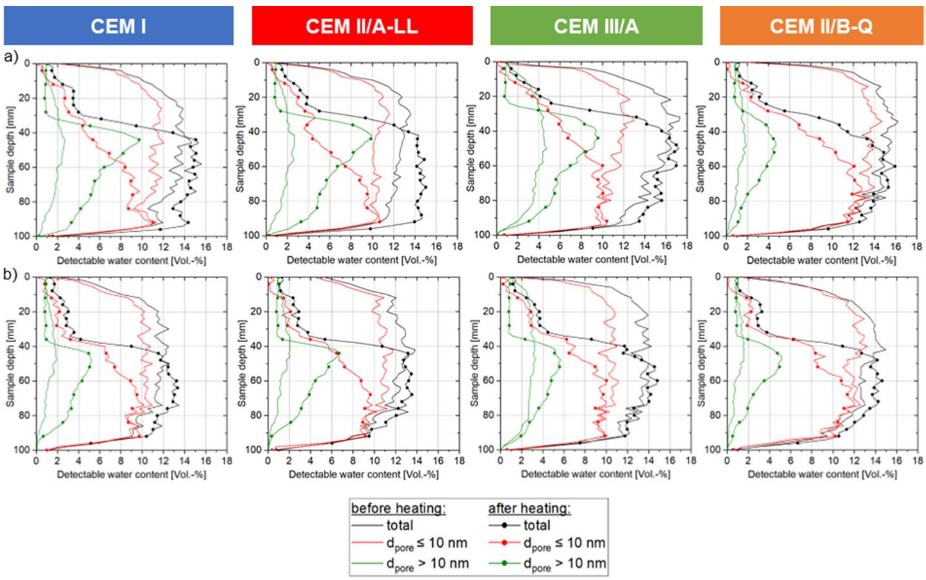

Fig. 4 1D moisture profiles with average pore size specific moisture distribution before and after one-sided heating **a** without PP fibers; **b** with PP fibers

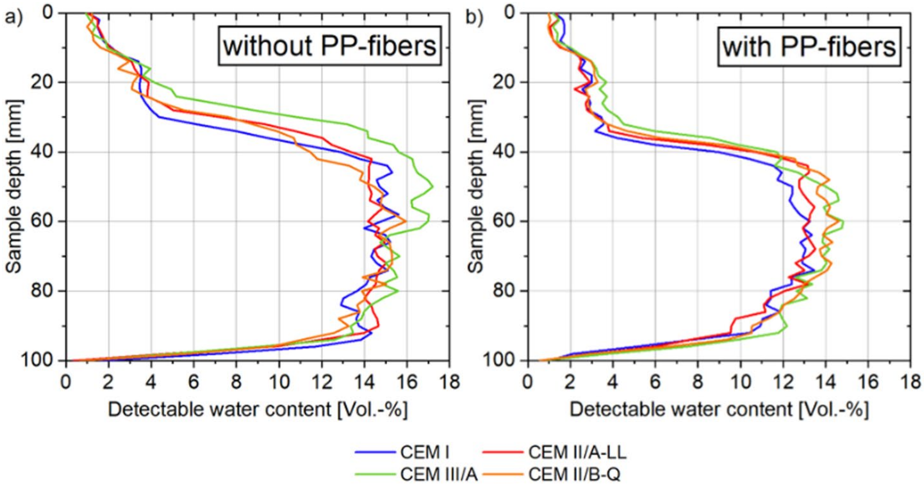

Fig. 5 1D moisture profile after heating **a** without PP fibers; **b** with PP fibers

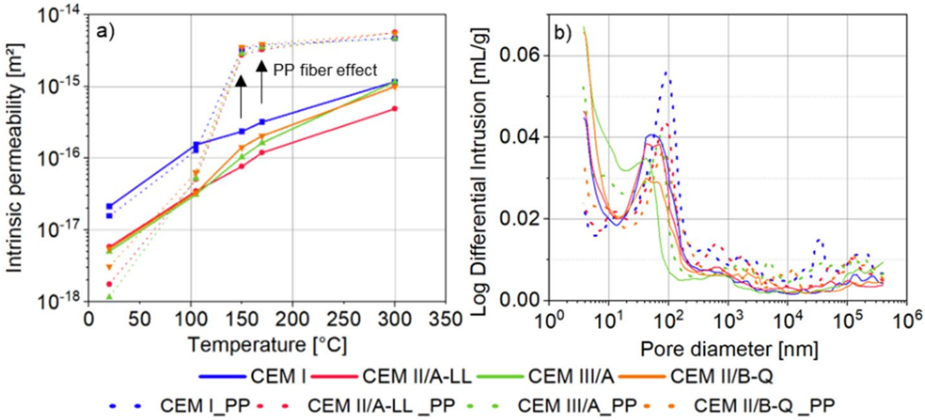

Fig. 6 **a** Average intrinsic gas permeability after exposure to 20, 105, 150, 170 and 300 °C showing the effect of the PP fibers on permeability development; **b** Average initial differential porosity

heating, all concretes showed a more advanced drying front with comparable drying gradients. Despite the fibers, the moisture clog was still detected within every sample at similar depths. This indicates that the transport properties in every type of concrete became equal with fiber addition at elevated temperatures and the cement type specific differences almost disappeared completely. A direct comparison between the 1D moisture profiles after heating for concrete with and without PP fibers is provided in Fig. 5.

The gas permeability measurements (see Fig. 6a) showed a higher initial permeability for CEM I concrete in comparison to blended cement concrete, with increasing temperature the permeability in all samples increased. However, at temperatures above 105 °C CEM III/A and CEM II/B-Q experienced a steeper permeability increase in comparison to CEM I and CEM II/A-LL. Therefore, the initial differences between CEM I and CEM III/A or CEM

II/B-Q concrete became less pronounced and ultimately vanished at 300 °C. This indicates that the permeability differences at elevated temperatures between these types of concrete are much smaller than in the initial state and therefore suggesting that the permeability alone might not be the only driving force responsible for the thermally induced moisture transport. The effectiveness of PP fibers is also visible in the development of permeability, where after exceeding temperatures of 105 °C the permeability suddenly increases to the same level in every type of concrete. Interestingly, the main permeability increase occurs at temperatures below the fiber melt starting at 150 °C, which has also been observed in other studies [28, 29].

The MIP results (Fig. 6b) showed a similar picture for CEM I and CEM II/A-LL concrete with equal pore size distributions. The CEM II/B-Q sample showed a similar course but more gel pores and less capillary pores. CEM III/A sample exhibited the lowest number of capillary pores over 30 nm but the highest number of small capillary and gel pores below this size. No major differences in the pore size distribution above 200 nm were recognized. The MIP measurements in PP fiber mixtures showed a slight increase in porosity and an overall pore coarsening effect in the initial state, however, the pore coarsening seemingly did not increase the initial permeability of PP fiber concrete.

3.3 Thermal Phase Decomposition

The ^{1}H-NMR measurements revealed that differences in moisture distribution cannot be attributed solely to variations in permeability. This is particularly evident in CEM III/A and CEM II/B-Q concretes, which, despite having similar initial moisture contents and permeabilities, exhibit markedly different moisture profiles after heating. These findings suggest that moisture distribution is strongly influenced by the decomposition and dehydration behavior of the respective cementitious pastes.

To investigate this further, the mineral phase composition and dehydration behavior were analyzed using XRD and TGA on hardened cement paste samples published in [16]. For the XRD analysis, nearly cubic specimens (ca. $4 \times 4 \times 4$ cm^3) were heated with 2 K/min to 105 °C, 300 °C, and 500 °C and held for 48 h. After heating, the samples were sealed in plastic foil and stored in a desiccator to prevent rehydration. Subsequently, the samples were broken, immersed in isopropanol, and ground into a fine powder using a McCrone mill. The measurements were performed using a Bruker D8 DaVinci device using Cu Kα radiation and a step width of 0.05° per second, covering a range from 5° to 80°. The obtained data was quantitatively evaluated by Rietveld refinement using TOPAS V7.0 software.

Figure 7 presents the phase composition before and after thermal exposure. Significant initial differences were observed. CEM I exhibited the highest content of AFt (Ettringite) and AFm phases (hemicarboaluminate, monocarboaluminate and monosulfoaluminate), approximately 11.6 wt.-%, whereas CEM II/A-LL, CEM III/A, and CEM II/B-Q showed contents between 8.5 and 9.0 wt.-%, respectively. Additionally, CEM I and CEM II/A-LL contained higher amounts of C-(A)-S-H and portlandite compared to CEM III/A and CEM II/B-Q. These differences are attributed to the lower Portland cement clinker content in the latter cements, resulting in reduced hydrate formation. Moreover, the pozzolanic reaction leads to the formation of C-(A)-S-H at the expense of portlandite. Calcium carbonate was detected in all samples, with particularly high quantities in CEM II/A-LL as expected. However, comparable amounts were also found in the other specimens. The presence of

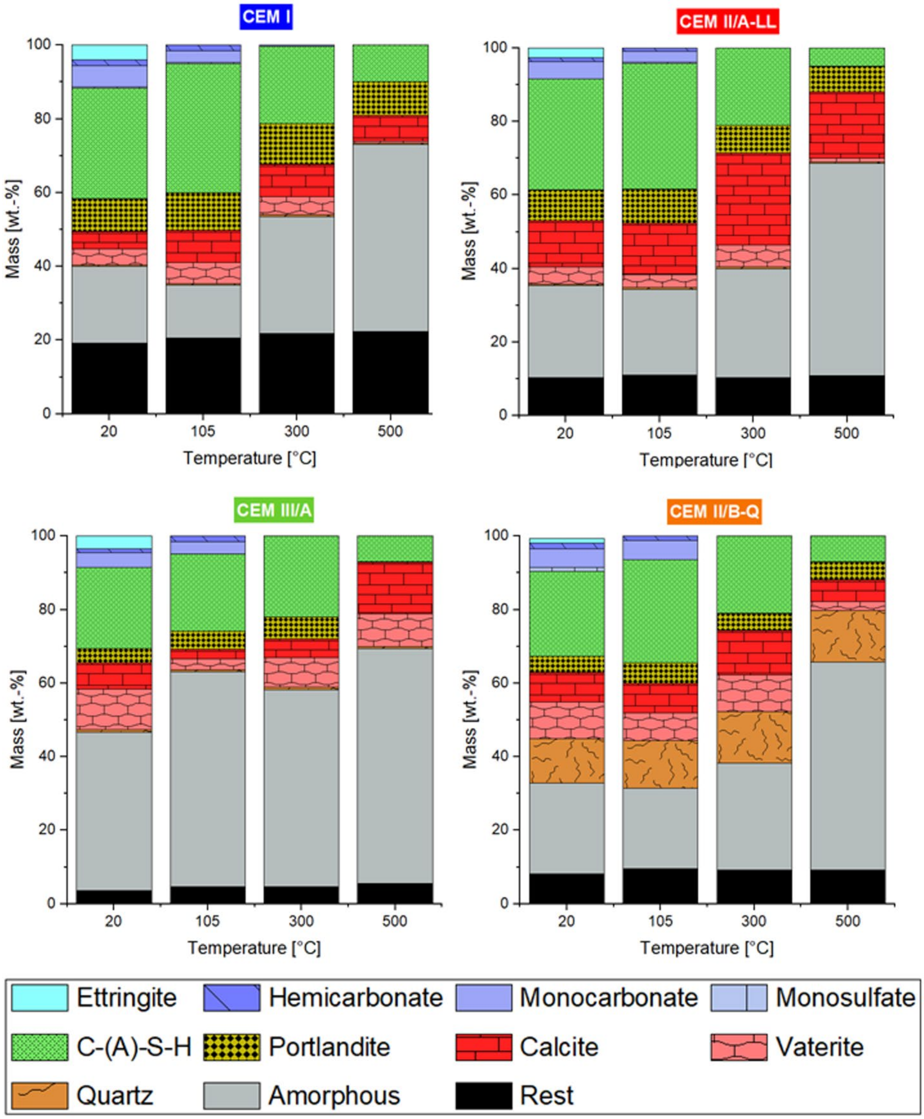

Fig. 7 Phase composition of the different hardened cement pastes after exposure to 20, 105, 300 and 500 °C determined by XRD Rietveld Analysis

significant quantities of vaterite suggests carbonation, especially in CEM III/A and CEM II/B-Q pastes, likely due to their lower portlandite contents [30, 31]. Furthermore, larger fractions of quartz were identified in the CEM II/B-Q sample which are a byproduct of calcined clay. Upon heating to 105 °C, decomposition of AFt phases was observed in all samples. Increasing the temperature to 300 °C led to further decomposition of AFm phases. In CEM I and CEM II/A-LL, C-(A)-S-H underwent significant decomposition at 300 °C and was nearly completely decomposed at 500 °C. In contrast, the C-(A)-S-H phases in CEM III/A and CEM II/B-Q remained largely stable up to 300 °C, with substantial decomposition only occurring at 500 °C. This indicates a higher thermal stability of the main hydrate phases in these cements. The dihydroxylation of C-(A)-S-H is primarily responsible for the increased amorphous content observed after exposure to 500 °C. Portlandite was still detectable even after heating to 500 °C, although its characteristic peaks in the XRD patterns showed reduced intensity and increased width, indicating a loss of crystallinity due to dehydration rather than complete structural degradation. This observation aligns with findings reported in the literature [32].

The TGA results presented in Fig. 8 were obtained using a Mettler Toledo instrument under nitrogen atmosphere, with a heating rate of 10 K/min up to 1000 °C. Due to the solvent exchange during sample preparation, no free evaporable water remained in the specimens.

The results indicate that CEM I exhibited the most pronounced mass loss associated with the decomposition of AFt and AFm phases within the temperature range of 70 to 200 °C, which is consistent with the XRD findings. In the case of CEM II/B-Q, a significant mass loss was attributed to the decomposition of AFm phases, most likely monocarboaluminate. CEM III/A showed the least mass loss overall, supporting the hypothesis that its main hydrate phase, C-(A)-S-H, is thermally more stable. Up to 300 °C, the highest mass loss was observed in CEM I, followed by CEM II/A-LL, CEM II/B-Q, and finally CEM III/A. Beyond 300 °C, the decomposition of portlandite was detected, with the highest contents found in CEM I and CEM II/A-LL, again in agreement with the XRD results. Starting at approximately 500 °C, the decomposition of calcium carbonate was observed, continuing up to around 760 °C. Notably, a two-stage decomposition process was identified: the first peak corresponds to the breakdown of amorphous and poorly crystalline vaterite, while the second peak represents the decomposition of calcite. The highest relative mass loss in this temperature range was recorded for CEM II/A-LL, due to its initially high calcite content. Pozzolanic and latent hydraulic binders also exhibited significant mass loss, attributed to carbonation and subsequent decomposition of calcium carbonate phases.

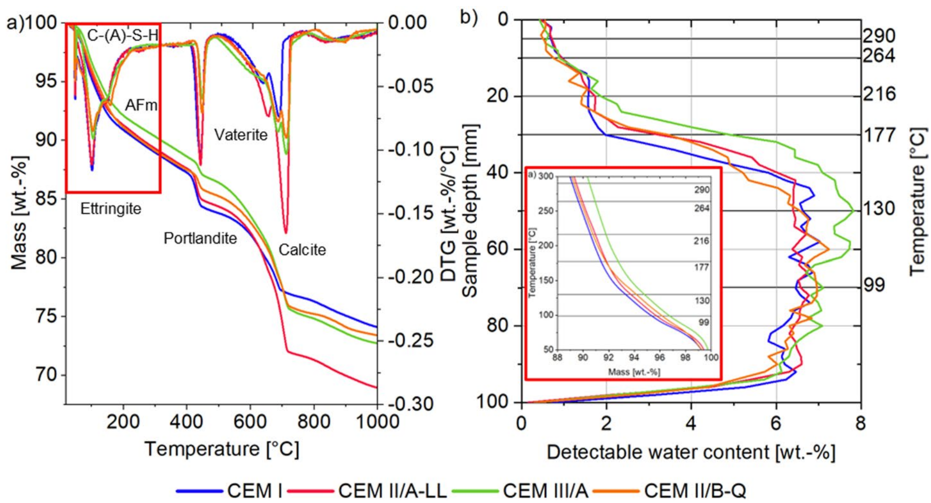

Fig. 8 **a** Dehydration behavior of the different cement pastes **b** comparison between mass loss in cement paste (TGA) and the drying behavior after one sided heating (^{1}H-NMR) showing the same sequence of mass loss up to 300 °C (10 K/min)

A comparison between the TGA and ^{1}H-NMR moisture profiles recorded after heating show the same sequence of mass loss and drying, respectively (see Fig. 8). This shows that the thermally induced moisture distribution and the development of the drying front plus moisture clog is highly dependent from the dehydration behavior of the cementitious matrix. Concluding that the permeability alone is not sufficient to describe the moisture transport in concrete.

4 Discussion

The results of this study clearly demonstrate that the type of cement significantly influences the spalling behavior of concrete. The lowest spalling susceptibility was observed in CEM I concrete, which can be attributed to its high permeability, low moisture content, and efficient water release during high-temperature exposure. This combination results in a reduced amount of energy stored in the form of hot water, allowing much of it to escape early during a fire event. Although CEM III/A and CEM II/B-Q concretes exhibit similar permeability to CEM I at elevated temperatures, this factor appears to play a minor role. TGA indicates that the majority of water is released between 50 °C and 170 °C, suggesting that permeability at lower temperatures is more critical for effective water release. In CEM III/A and CEM II/B-Q concretes, higher initial moisture content and restricted evaporation lead to greater energy availability, thereby increasing the risk of spalling. CEM II/A-LL concrete, which shows the lowest permeability across the entire temperature range, also presents a potential spalling risk. However, its moisture distribution and dehydration behavior closely resemble those of CEM I, indicating that transport properties may be more influential than moisture content alone.

Nevertheless, the results are consistent with current findings regarding spalling mechanisms proposed by Yarmohammadian and Felicetti [33], which emphasize the importance of sufficient thermal energy and water during crack initiation for the severity of spalling. A coherent representation of the conducted investigations normalized over the sample depth of the one-sided heated cylinders is given in Fig. 9. Here it can be distinguished between a dry, moist and saturated zone (‘’moisture clog’’). The dry zone refers to the region up to the point where moisture content begins to rise sharply, marking the start of the moist zone. This moist zone extends until the onset of the moisture clog, which is defined as the intersection between the water content after heating with the initial state before heating. The measured temperature distribution within the specimens is consistent across all cement types. Therefore, it can be stated that there are no significant differences in thermal conductivity or heat capacity among the different concrete types, which may influence spalling. Nevertheless, due to reduced dehydration and lower permeability, blended cement concrete retains higher water content in the moist zone prior to the beginning of the moisture clog developed at temperatures between 150 and 230 °C. This fits well with the fire tests in which spalling began to occur at concrete temperatures between 170 and 240 °C [14]. Therefore, it can be concluded that the greater amount of available thermal energy in the form of hot water in concrete made with blended cements, significantly increases the risk of explosive spalling. In concretes containing PP fibers, the drying zone extends deeper due to increased permeability. As a result, the moist zone becomes thinner and shifts further inward, where lower temperatures prevail. Due to the uniformly increased permeability across all con-

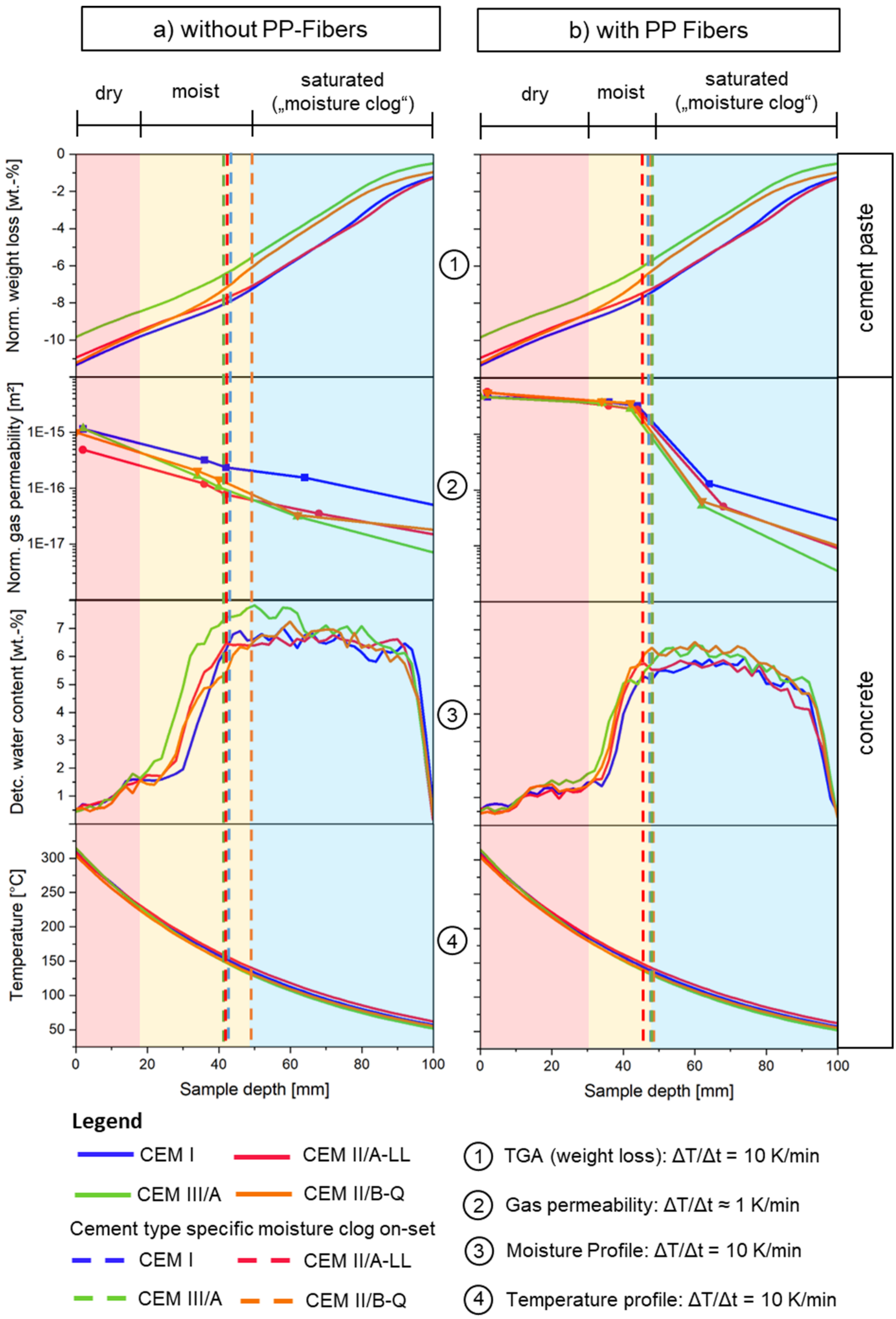

Fig. 9 Coherent representation of the investigations carried out with regard to dehydration behavior, gas permeability, moisture distribution, and temperature distribution after 70 min normalized over the sample length in different types of concrete **a** without PP fibers; **b** with PP fibers

crete types, moisture differences become much smaller and almost disappear. Although the drying sequence is influenced by permeability, it still matches the sequence of weight loss in the cement paste, as phase decomposition occurs independently of permeability. Because moisture availability is now significantly reduced in areas with lower temperatures (approximately 125–175 °C), spalling no longer occurs, as insufficient thermal energy can accumulate to cause damage. It should be noted that the temperature profiles presented in Fig. 9 were only measured in concrete without PP fibers but previous investigations with the same test set-up showed that the influence of PP fibers on the temperature development is neglectable [34].

The presented results show clearly why blended cement concrete is more prone to spalling than conventional concrete. However, the differences in spalling susceptibility between the single blended cement concrete types are still not fully understood.

Interestingly, CEM II/B-Q concrete exhibited the most severe spalling, despite behaving similarly to CEM III/A in many respects. The temperature measurements showed no significant differences, indicating that the thermal conductivity and heat capacity of the investigated materials are comparable. With similar temperature evolution and distribution during heating, no significant differences in dehydration kinetics are expected as shown by the TGA and XRD data. This suggests that additional thermohydraulic or thermomechanical factors must be contributing. Notably, CEM II/B-Q concrete contained significantly more gel pore water compared to the other mixes. This raises the question of whether pore size distribution influences pore pressure. First indications in this direction are given by Jiang et al. [35] who found that pore pressure increases with decreasing porosity and pore radius in unsaturated pores, potentially explaining the heightened spalling in CEM II/B-Q concrete.

In addition to thermohydraulic effects, potential thermomechanical contributions may also be responsible for the observed differences in spalling behavior. Since the majority of the concrete volume consists of aggregates, it can be assumed that no significant differences arise in terms of the stresses caused by restrained thermal expansion for the tested concretes with different cements. Furthermore, as the stiffness of concrete is largely governed by the aggregates too, the effects of the cement paste dehydration can be considered minor as described by Peters et al. [36]. Nevertheless, mineralogical differences may also contribute to the observed behavior through other underlying mechanisms. The enhanced thermal stability of C-(A)-S-H phases in CEM II/B-Q and CEM III/A could alter thermomechanical responses, particularly regarding load-induced thermal strains (LITS). In restrained concrete structures, LITS can be beneficial, as they develop in the direction of the applied load and help reduce compressive stresses caused by restrained thermal expansion [37], potentially lowering the risk of spalling. LITS primarily result from thermal transient creep and drying creep, both of which are closely linked to the decomposition of hydrate phases and associated water transport [38, 39]. Peters et al. [36] observed that the progression of C-S-H dehydration closely aligns with the development of LITS, attributed to creep-like sliding of C-S-H under compressive stress. However, the thermally stable C-(A)-S-H phases in CEM II/B-Q and CEM III/A may inhibit this sliding, leading to reduced LITS and lower stress relaxation, ultimately increasing spalling susceptibility. In addition to LITS, the differing dehydration behavior of the cement types may influence the thermal mismatch between the shrinking hardened cement paste and the expanding aggregates during heating. Koyama et al. [40] describe the shrinkage behavior of pure cement paste as a sequence of four characteristic stages. In the initial stage (20 °C to 140 °C), shrinkage is triggered by the evaporation of free water and the decomposition of AFt phases. This is followed by a more moderate shrinkage regime between 140 °C and 300 °C, mainly governed by the release of interlayer water from the C–S–H structure. Beyond this range, from 300 °C to 490 °C, shrinkage intensifies markedly due to continued dehydration of C-S-H and especially portlandite. Based on the presented TGA and XRD results, it can be assumed that hardened cement paste of CEM I exhibits more pronounced shrinkage than the blended cements, as it contains higher amounts of AFt and AFm phases as well as portlandite, all of which significantly contribute to shrinkage. However, spalling was least pronounced for CEM I, indicating that, in this case, the effect of shrinkage and thermal mismatch does not appear to be a dominant factor. Nonetheless, in addition to the hydration phases, the residual mineralogical composition of the cementitious matrix should not be disregarded, as it may lead to thermal mismatch between hydrate and non-hydrate phases at the binder scale. XRD analysis revealed high quartz content in CEM II/B-Q concrete, which acts in a further sense as very fine aggregate. The thermal mismatch between the cement paste and quartz can generate internal stresses that promote spalling. This mismatch is particularly pronounced for quartz but also applies to limestone and unreacted slag, which are present in significant quantities in CEM II/A-LL and CEM III/A, potentially further increasing the risk of explosive spalling in comparison to CEM I concrete.

The addition of 2 kg/m³ of PP fibers effectively prevented spalling in all concrete types, primarily due to the uniform increase in permeability at elevated temperatures. This demonstrates that a viable solution to the heightened spalling risk in blended cement concretes already exists, albeit at the expense of reduced workability in the fresh concrete state. For concrete with CEM I, omitting PP fibers may be considered to preserve workability. This is supported by the apparently sufficient permeability, which results in only minimal spalling and moderate temperature increases within the structural member due to adequate concrete cover. Due to the low permeability of blended cement concretes, severe spalling occurs, resulting in significant temperature increases endangering the structural integrity of the component. Consequently, the incorporation of PP fibers is necessary to provide sufficient permeability and enable reliable moisture release to avoid spalling during fire exposure. However, further investigations are required to assess whether the same fiber dosage with larger diameters (e.g., d = 32 µm), resulting in a lower number of fibers at the same volumetric content, or reduced fiber dosages, can provide sufficient protection while minimizing the negative impact on workability. If this is not the case with conventional fibers, the next step could be the introduction of altered PP fibers, which are known to be much more effective [41]. As these aspects were not investigated in this study, no definitive recommendations regarding fiber size, dosage and type can be provided at this stage. However, these considerations are particularly relevant for the use of calcined clay cement, which further compromise workability. Therefore, combining PP fibers with calcined clays may present significant practical challenges for concrete technology.

The findings of this study highlight that the use of blended cements in applications where fire protection is of paramount importance should be carefully evaluated, even in NSC. At present, Eurocode 2 does not provide provisions addressing the use of blended cements in relation to fire-induced spalling. However, further comprehensive and in-depth research is required to fully understand the influence of cement type and to establish well-founded regulations.

5 Conclusion

This research project investigated the impact of blended cements on the spalling behavior of normal strength concrete. The study included a comprehensive literature review, spalling experiments, and the characterization of moisture distribution, transport mechanisms, and dehydration behavior of various cement pastes. The following conclusions were drawn:

- **State of the art**: The literature review of the current state of the art revealed that cement type significantly influences the spalling susceptibility of concrete. However, the number of studies featuring well-defined testing procedures and comprehensive material characterization still remains limited. Moreover, comparisons between different research groups proved to be challenging due to the lack of standardized testing protocols. As a result, clear trends could only be identified for SF, MK, and high volumes of FA (>25%). While SF and MK tend to increase spalling susceptibility, high-volume FA appears to reduce it.
- **Spalling Susceptibility**: The use of CEM II/A-LL, CEM III/A, and particularly CEM II/B-Q increased the spalling susceptibility. This is attributed to higher water retention at elevated temperatures, resulting from high initial moisture contents, reduced permeability and a more thermally stable cementitious matrix in blended cement concretes. Thus, the amount of available energy in the form of hot water increases in the area ahead of the moisture clog at temperatures where spalling occurred (170–240 °C). The differences in spalling behavior among the individual blended cements are not yet fully understood. Potential influencing factors include pore-size-specific moisture distribution and the specific mineral phase composition, which may affect thermomechanical properties. The increased tendency for spalling in concretes with lower clinker content, despite their environmental benefits, must be carefully considered in future construction practices, especially in tunnel construction.
- **Effectiveness of PP Fibers**: The incorporation of 2 kg/m^3 of PP fibers effectively prevented explosive spalling across all cement types. Therefore, sufficient concrete cover remained to protect a potential reinforcement layer from direct flame exposure and consequent strength loss. PP fibers thus remain a reliable mitigation strategy. However, further research is needed to determine whether lower fiber dosages could be sufficient, especially in systems containing calcined clay, where higher fiber content adversely affects workability.

Acknowledgements We gratefully acknowledge the support of the German Research Foundation (DFG) and extend our sincere thanks for their financial support throughout the joint project “Thermohydraulic spalling mechanisms in concretes with different binders with and without PP fibers under fire exposure: An experimental and numerical analysis” (Project No. 491928256). We also express our deep appreciation to our project partner, Ruhr University Bochum, for their outstanding collaboration. Special thanks are extended to our colleagues at BAM, in particular the teams from divisions 6.3: Structure Analysis, 7.1: Building Materials, and 7.4: Technology of Construction Materials. Their expertise and resources have significantly enriched the scope and depth of this study.

Author Contributions T: P.: Conceptualization, Investigation, Formal analysis, Visualization, Writing – original draft, Writing – review & editing. F.D.: Supervision, Writing – review & editing. F.W.: Conceptualization, Resources, Funding acquisition, Project administration, Supervision, Writing – review & editing. L.S.: Conceptualization, Resources, Funding acquisition, Project administration, Supervision, Writing – review & editing.

Funding Open Access funding enabled and organized by Projekt DEAL.

Data Availability Data will be made available on request.

Declarations

Conflict of interest The authors declare that they have no known competing financial interests, personal relationships or any other affairs that could have appeared to influence the work reported in this paper.

References

1. Fehérvári S (2008) Characteristics of Tunnel fires. Concr Struct 56–60
2. Schneider M (2019) The cement industry on the way to a low-carbon future. Cem Concr Res. https://doi.org/10.1016/j.cemconres.2019.105792
3. Scrivener KL, Vanderley JM, Gartner EM (2018) Eco-efficient cements: Potential economically viable solutions for a low-CO2 cement-based materials industry. Cem Concr Res 114:2–26. https://doi.org/10.1016/j.cemconres.2018.03.015
4. Shorter GW, Harmathy TZ (1961) Discussion on the Fire-resistance of prestressed concrete beams. 313–315
5. Felicetti R, Yarmohammadian R, Dal Pont S et al (2024) Fast vapour migration next to a depressurizing interface: a possible driving mechanism of explosive spalling revealed by neutron imaging. Cem Concr Res. https://doi.org/10.1016/j.cemconres.2024.107508
6. Bažant ZP, Cusatis G (2005) Concrete creep at high temperature and its interaction with fracture: Recent progress. CONCREEP 7: Nantes 449–460
7. Schneider U (1982) Behaviour of Concrete at High Temperatures. Deutscher Ausschuss für Stahlbeton, pp 1–110
8. Bažant ZP (1997) Analysis of Pore Pressure, thermal Stredd and Fracture in Rapidly Heated Concrete. International Workshop on fire Performance of High-Strength Concrete: Gaithersburg
9. Ulm FJ, Coussy O, Bazant ZP (1999) The "Chunnel" fire I: chemoplastic softening in rapidly heated concrete. J Eng Mech 125:272–282. https://doi.org/10.1061/(ASCE)0733-9399(1999)125:3(272)
10. Pistol K, Weise F, Meng B et al (2011) The mode of action of polypropylene fibres in high performance concrete at high temperatures. 2nd International RILEM Workshop on Concrete Spalling due to Fire Exposure: Delft, The Netherlands 289–296
11. Pittrich T, Weise F, Stelzner L (2025) The impact of blended cements on the spalling behavior of concrete at elevated temperatures: a review. Mater Struct. https://doi.org/10.1617/s11527-025-02713-x
12. Pimienta P, McNamee R, Hager I et al (2023) Recommendation of RILEM TC 256-SPF on the method of testing concrete spalling due to fire: material screening test. Mater Struct. https://doi.org/10.1617/s11527-023-02202-z
13. Pimienta P, McNamee R, Hager I et al (2024) Recommendation of RILEM TC 256-SPF on fire spalling assessment during standardised fire resistance tests: complementary guidance and requirements. Mater Struct. https://doi.org/10.1617/s11527-023-02248-z
14. Pittrich T, Stelzner L, Weise F (2024) Fire-induced spalling of normal strength concrete with different types of blended Portland cement. The 13th International Conference on Structures in Fire: Coimbra, Portugal 451–461
15. DIN EN 197-1 (2011) Cement-Part 1: Composition specifications and conformity for common cements. Beuth Ver lag GmbH, Berlin

16. Pittrich T, Jansen D, Weise F et al (2026) Thermal decomposition in blended cement systems and its effect on fire-induced concrete spalling: insights from XRD and TGA. Case Stud Constr Mater. https://doi.org/10.1016/j.cscm.2026.e05784
17. Eurocode 2 (2010) Design of concrete structures - Part 1–2: General rules - Structural fire design; German version EN 1992-1-2:2004+AC:2008. Beuth Verlag GmbH, Berlin
18. Klimek A, Stelzner L, Hothan S et al (2024) Influence of thermal strain on concrete spalling. Mater Struct. https://doi.org/10.1617/s11527-023-02274-x
19. Ozawa M, Tanibe T, Kamata R et al (2018) Behavior of ring-restrained high-performance concrete under extreme heating and development of screening test. Constr Build Mater 162:215–228. https://doi.org/10.1016/j.conbuildmat.2017.11.144
20. Maier M, Zeiml M, Lackner R (2020) On the effect of pore-space properties and water saturation on explosive spalling of fire-loaded concrete. Constr Build Mater. https://doi.org/10.1016/j.conbuildmat.2019.117150
21. Kruschwitz S, Munsch S, Telong M et al (2023) The NMR core analyzing tomograph: a multi-functional tool for non-destructive testing of building materials. Magn Reson Lett 3:207–219. https://doi.org/10.1016/j.mrl.2023.03.004
22. Hiller T, Costabel S (2025) NUCLEUS – a Matlab-based graphical user interface for forward and inverse modelling of NMR relaxometry data. SoftwareX. https://doi.org/10.1016/j.softx.2025.102447
23. Pittrich T, Peters S, Meschke G et al (2026) Thermally induced moisture transport in concrete with different types of blended Portland cement studied by 1H-NMR relaxometry. Mater Struct. https://doi.org/10.1617/s11527-026-03025-4
24. Stelzner L, Powierza B, Oesch T et al (2019) Thermally-induced moisture transport in High-Performance Concrete studied by X-ray-CT and ^{1}H-NMR. Constr Build Mater 224:600–609. https://doi.org/10.1016/j.conbuildmat.2019.07.065
25. International Organization for Standardization (2016) Evaluation of pore size distribution and porosity of solid materials by mercury porosimetry and gas adsorption - Part 1: Mercury Porosimetry (ISO Standard No. 15901-1)
26. RILEM TC 116-PCD (1999) RILEM TC 116-PCD: Permeability of Concrete as a Criterion of its Durability. Mater Struct 32:174–179
27. Klinkenberg LJ (1941) The Permeability of Porous Media to Liquids and Gases. Production Practice: 200–213
28. Muhammed A, Carre H, La Borderie C et al (2025) Influence of Polypropylene Fibers on Thermal-Induced Permability Changes in Concrete. 12th Int Conf Fract Mech Concrete Concrete Struct Vienna Austria. https://doi.org/10.21012/FC12.1244
29. Bošnjak J, Ožbolt J, Hahn R (2013) Permeability measurement on high strength concrete without and with polypropylene fibers at elevated temperatures using a new test setup. Cem Concr Res 53:104–111. https://doi.org/10.1016/j.cemconres.2013.06.005
30. Lollini F, Redaelli E (2021) Carbonation of blended cement concretes after 12 years of natural exposure. Constr Build Mater 276. https://doi.org/10.1016/j.conbuildmat.2020.122122
31. Bucher R, Diedrich P, Escadeillas G et al (2017) Service life of metakaolin-based concrete exposed to carbonation Comparison with blended cement containing fly ash, blast furnace slag and limestone filler. Cem Concr Res 99:18–29. https://doi.org/10.1016/j.cemconres.2017.04.013
32. Song H, Jeong Y, Bae S et al (2018) A study of thermal decomposition of phases in cementitious systems using HT-XRD and TG. Constr Build Mater. https://doi.org/10.1016/j.conbuildmat.2018.03.001
33. Yarmohammadian R, Felicetti R (2025) From Crack Initation To Instability At High Temperature: A Two Stage Mechanism For Fire-Induced Spalling in Concrete. 12th International Conference on Fracture Mechanics of Concrete and Concrete Structures: Vienna, Austria
34. Stelzner L (2021) Analyse des thermisch induzierten Feuchtetransports in gefügedichten Beton. Dissertation. University of Stuttgart
35. Jiang W, Zhang D, Zheng X et al (2023) Development of pore pressure in cementitious materials under low thermal effects: evidence from optimization of pore structure by incorporation of fly ash. Materials (Basel). https://doi.org/10.3390/ma16124214
36. Peters S, Vu G, Meschke G (2025) A multiscale model for predicting the Young's modulus and the thermal-expansion coefficient of concrete at high temperatures. Constr Build Mater 479. https://doi.org/10.1016/j.conbuildmat.2025.141259
37. Torelli G, Mandal P, Gillie M et al (2016) Concrete strains under transient thermal conditions: A state-of-the-art review. Eng Struct 127:172–188. https://doi.org/10.1016/j.engstruct.2016.08.021
38. Schneider U (1988) Concrete at High Temperatures -- A General Review. Fire Saf J 13:55–68. https://doi.org/10.1016/0379-7112(88)90033-1
39. Bazant ZP, Xi Y (1994) Drying creep of concrete: constitutive model and new experiments separating its. Mech Mater Struct 27:3–14

40. Koyama T, Ozawa M, Kanematsu M (2024) Study on the thermal shrinkage behavior of cement paste under high temperature envirnoment. Cem Sci Concrete Technol 78:128–136. https://doi.org/10.14250/cement.78.128
41. Weise F, Stelzner L, Weinberger J et al (2017) Influence of the pre-treatment of PP-fibres by means of electron irradiation on the spalling behaviour of High-Strength Concrete. 5th International Workshop on Concrete Spalling: Boras, Sweden 345–358

Authors and Affiliations

Tim Pittrich[1,2] · Frank Dehn[2] · Frank Weise[1] · Ludwig Stelzner[1]

✉ Tim Pittrich
tim.pittrich@bam.de

✉ Ludwig Stelzner
ludwig.stelzner@bam.de

Frank Dehn
frank.dehn@kit.edu

Frank Weise
frank.weise@bam.de

1 Federal Institute For Materials Research and Testing, Berlin, Germany

2 Karlsruhe Institute of Technology, Karlsruhe, Germany